Partial Symmetry Detection for 3D Geometry using Contrastive Learning with Geodesic Point Cloud Patches

Gregor Kobsik   Isaak Lim   Leif Kobbelt

Visual Computing Institute, RWTH Aachen University

Abstract

Symmetry detection, especially partial and extrinsic symmetry, is essential for various downstream tasks, like 3D geometry completion, segmentation, compression and structure-aware shape encoding or generation. In order to detect partial extrinsic symmetries, we propose to learn rotation, reflection, translation and scale invariant local shape features for geodesic point cloud patches via contrastive learning, which are robust across multiple classes and generalize over different datasets. We show that our approach is able to extract multiple valid solutions for this ambiguous problem. Furthermore, we introduce a novel benchmark test for partial extrinsic symmetry detection to evaluate our method. Lastly, we incorporate the detected symmetries together with a region growing algorithm to demonstrate a downstream task with the goal of computing symmetry-aware partitions of 3D shapes. To our knowledge, we are the first to propose a self-supervised data-driven method for partial extrinsic symmetry detection.

Figure 1. Examples of symmetric regions after applying our symmetry detection and region growing method. The top row uses our SymCL and bottom row our SymML model. Colors represent different regions within detected symmetries, where dark shades represents the initially detected partial symmetries and the light ones are completed regions after applying a region growing algorithm to them. Note how the same input shape can lead to multiple valid solution.

1. Introduction

Symmetry detection in 3D geometry is a challenging task, which has already been studied for many years. The extraction of symmetry information is highly beneficial in the domain of computer vision and computer graphics for various downstream tasks, e.g. 3D geometry completion, segmentation, hierarchical decomposition, compression or shape matching, structure-aware meshing and procedural generation. There are various solutions, including model-driven and learning-based methods, for global extrinsic symmetry detection. However, research on partial extrinsic symmetry detection, also called self-similarity, has not received the same level of attention in recent years. Note that the problem of detecting partial symmetries is ambiguous, since multiple valid solutions for almost any input can exist (see Fig. 1).

Classical methods mostly rely on hand-crafted features and model-driven algorithms to detect symmetries. However, these approaches are often highly susceptible to parameter tuning, with manually selected values applicable only to specific shapes, hence rendering them unreliable in general. To illustrate the challenging nature of the problem, consider two symmetric regions A and B. We can assess if those regions expose extrinsic symmetry with respect to each other in three steps: i) A valid registration of region A to B must be found to align both regions. ii) Next, a distance between the regions can be calculated. iii) Given a predefined distance threshold it can be determined if they exhibit a symmetric relationship or not. I.e. A and B are symmetric to each other if $d(A, B) < \epsilon$. Even though this approach seems straightforward, it is far from trivial in practice due to the fact that 3D geometry comprises infinitely many coherent subregions, which might exhibit some kind of symmetry with respect to each other. We can quantize the given geometry into a finite number of n local subsets. Even in this setup each candidate needs to be compared with each other candidate resulting in an $O(n^2)$ complexity, where finding valid registrations is a time-consuming step.

Our aim is to find symmetric regions of maximal size

within a shape. To circumvent the time-consuming registration process we propose to learn rotation, reflection, translation and scale invariant features describing local geodesic patches of a shape through contrastive learning and compare them in latent space. Thereafter, we obtain a distance matrix from which possibly multiple symmetric regions can be extracted. We show that the learned features are robust and generalize well to all geometry classes and multiple datasets without any adjustments.

Note that previous model-driven methods remain mostly inaccessible with no publicly available implementations. We could not identify any data-driven approaches for partial extrinsic symmetry detection. Additionally, there exists no benchmark test for partial extrinsic symmetry detection, which makes it difficult to compare different methods.

2. Related Work

Mitra et al. [21] offer an comprehensive survey of classical model-based approaches and provide an extensive overview on the background of symmetry analysis in 3D geometry. As stated there, most organic as well as man-made objects exhibit some kind of symmetry, which can be analyzed and possibly extracted.

Global Reflective Symmetry One predominant kind of symmetry is the global reflective symmetry. It has been studied long before in the 2D domain [1] and many classical algorithms have been proposed for the detection of reflective planes in 3D based on Fourier descriptors [11], generalized even moments [17], randomized voting techniques [27] or viewpoint entropy distribution [13]. Some of these approaches even aim at detecting global symmetry with missing geometry [31]. In recent years novel learning-based techniques emerged, either supervised [10] or unsupervised [9, 15]. Although these approaches are able to surpass the performance of classical model-based methods and deal robustly even with incomplete data, they aim at detecting only global reflective and not partial symmetries within 3D geometry.

Extrinsic Partial Symmetry There exist classical model-based work that deals with the analysis of 3D shapes and the extraction of extrinsic partial symmetry, either based on geometric hashing [7], voting techniques in the transformation space [19, 26], matching feature lines [3] or directly in the space of correspondences [16]. Mitra et al. [21] abstract those techniques into three stages consisting of feature selection, aggregation and extraction. Our work is inspired by this analysis, but aims at including the generalization capabilities of neural networks to improve upon them.

Intrinsic Symmetry Another kind of symmetries encountered in 3D geometry are intrinsic symmetries, which are characterized by being invariant to isometric transformations, e.g. pose-independent symmetries in human bod-

ies. Both global [25, 33] and partial [20, 24, 34, 35] intrinsic symmetry detection methods have been proposed in the past. Recently Qiao et al. [29] proposed a supervised approach that learns to detect intrinsic symmetries based on examining the eigenfunctions of the Laplace-Beltrami operator. Since intrinsic symmetries are relevant only in specific settings with isometric deformations (like human poses), we focus on extrinsic partial symmetries, which cover all setting with rigid or articulated 3D models. Furthermore, our method can be trained in a self-supervised manner.

Part Relationships In the domain of shape encoding and generation [8, 14, 22, 36, 37] some methods incorporate symmetric relationships into the hierarchical structure of shapes to regularize the encoding capabilities of their networks. Unfortunately, these methods are not designed to detect and extract symmetry information and can only decode them from a learned latent space. Mo et. al [22] describe that the mapping to this latent space can be learned by a second encoder trained only on point clouds, and thus symmetric relationships can be recovered by the pretrained decoder. Unfortunately, our experiments (see supplementary material Sec. 8) show that this approach does not generalize well to inputs outside the training set. In contrast, our method is more general as it does not require labeled ground truth data. Furthermore, it is not limited to a single class of pretrained shapes and works well with arbitrary complex input geometry.

3. Learning Partial Extrinsic Symmetries

In this section we present our symmetry detection method, which is to the best of our knowledge the first self-supervised data-driven approach that detects partial extrinsic symmetries. Our symmetry detection pipeline can be split into three stages i) feature learning, ii) aggregation and iii) symmetry extraction, which are described in more detail in the following subsections (see Fig. 2). In the first stage we implement a learning-based technique to acquire robust and transferable features capable of capturing the local neighborhood of a sample point. Secondly, we cluster these features in the latent space to aggregate the symmetry information. Using a single dot-product computation, we can efficiently assess how geometrically similar two regions are to each other. As our learned features are rotation, reflection, translation and scale invariant, we consider the similarity of regions under all those transformations in the latent space. Lastly, we extract partial symmetries by computing connected components based on the local neighborhood of clustered features, cast back into the 3D space of the input geometry.

3.1. Geodesic Patches

To enable partial extrinsic symmetry computation, we must discretize the continuous surface of a 3D geometry into lo-
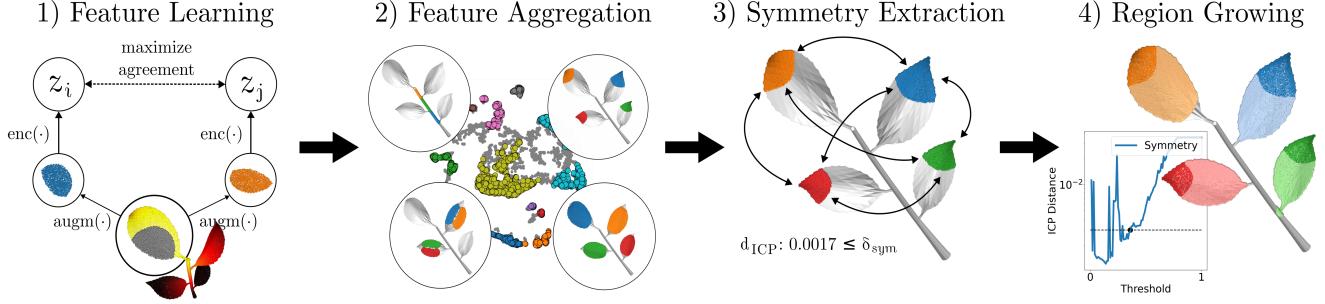
Figure 2. Overview of our method to extract maximal regions of extrinsic partial symmetry. 1) We learn features invariant to rotation, reflection, translation and scaling using geodesic patches. 2) After the training, we compare local patches in the latent space and aggregate symmetry information through clustering. 3) Symmetries are extracted from the 3D geometry and their quality evaluated by the ICP distance. 4) We complete the symmetric regions by a region growing algorithm.

cal patches. Patch centers are selected via the farthest point sampling (FPS) of a point cloud of the input geometry. Typically, a ball-query per sample point is performed to extract a local region of the geometry [28]. We argue that the extraction method, which relies on Euclidean distances, is flawed as it fails to respect the intrinsic metric of the input surface (cmp. Fig. 3). To address the issue, we suggest calculating geodesic distances using the heat method [4, 30] originating from the patch centers and identifying the closest neighbors within a fixed distance δ_d or a predefined number of points δ_n. This directly determines the size of the patch.

In our work we discretize each input geometry mesh using uniform sampling into a point cloud consisting of 2^{16} points, from which we select 2^{11} patch centers using FPS. For each patch center, geodesic patches p of multiple sizes $\delta_n = [2^9, 2^{10}, 2^{11}, 2^{12}, 2^{13}]$ are chosen to consider symmetries at various scales.

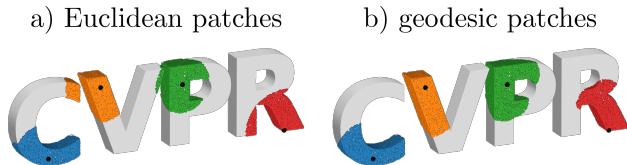a) Euclidean patches   b) geodesic patches

Figure 3. Comparison between Euclidean and geodesic patches. Note how the orange and red Euclidean patches do not respect the connectedness and the intrinsic metric of the surface, respectively.

3.2. ICP Distance

As previously mentioned, we may assess the symmetry of two shapes in relation to each other by initially registering them with one another and subsequently calculating the distance between them. For the sake of completeness, we describe a distance measure for point clouds that is invariant to transformations from the orthogonal group $O(3)$, which we call the ICP distance. Given two point clouds A and B:

1) Register A onto B using the iterative closest point (ICP) algorithm [2]. 2) Compute the two-sided Chamfer distance d_{CD} [6] between the aligned point clouds A_{ICP} and B.

$$d_{CD}(A, B) = \frac{1}{|A|} \sum_{a \in A} \min_{b \in B} \|a-b\|^2 + \frac{1}{|B|} \sum_{b \in B} \min_{a \in A} \|a-b\|^2 \tag{1}$$

As the ICP algorithm is highly sensitive to the initialization, we suggest repeating the registration process several times, centering the point clouds around their mean $T_{mean}(\cdot)$, and applying a random rotation and reflection $R_{rand}(\cdot)$ to A each time. We define the smallest distance across all runs as the ICP distance d_{ICP}. As a compromise between consistency and speed we suggest employing $N = 30$ separate registrations, with a maximum of 100 iteration steps each. The ICP algorithm returns estimated rotation R and translation T ignoring scaling. Furthermore, we apply the farthest point sampling (FPS) $fps(\cdot)$ to the point cloud to restrict its size to 512 points. This speeds up the computation greatly and makes the distance comparable across inputs consisting of different number of points.

$$d_{ICP}(A, B) = \min_{i \in N} d_{CD}(A_{ICP,i}^{norm}, B^{norm}), \tag{2}$$

where

$$A^{norm} = T_{mean}(fps(A)), B^{norm} = T_{mean}(fps(B)) \tag{3}$$

$$R_i, T_i = ICP(R_{rand}(A^{norm}), B^{norm}) \tag{4}$$

$$A_{ICP,i}^{norm} = R_i T_i A^{norm} \tag{5}$$

Given this explicit measure of extrinsic similarity, local patches, regions, or parts can now be compared to each other and a distance matrix can be calculated to describe a shape's symmetry landscape.

3.3. Feature Learning

We aim to calculate the symmetry distance matrix in order to extract local symmetric patterns. The ICP distance could

be a good and reliable measure as already stated before. Comparing two inputs takes seconds, which is manageable when doing so for a few regions n. However, it becomes impractical due to the $O(n^2)$ complexity when aiming to cover the shape with a dense distribution of local patches. For example, it takes only 35 seconds to compute a 16×16 distance matrix, but almost 4 hours for an $1k \times 1k$ matrix and over 48 hours for a $5k \times 5k$ matrix. It is highly desirable to consolidate the comparison into a single operation. This goal can be achieved by lifting each patch p to a feature space and conducting the distance measurement with a dot-product operation. To embed local patches, we suggest training a neural network as a comprehensive feature extractor $enc(p^{norm}) = z$, where p^{norm} is the input patch represented as a point cloud consisting of 512 points and z the embedded vector with a dimension of 32.

Feature Invariance To account for various types of symmetry, we must calculate features that remain unaffected by rotation, reflection, translation and scale. We achieve rotation-invariance by utilizing Vector Neurons [5] at the core of our model. We use VN-DGCNN as the formulation of a lightweight feature encoder $enc(\cdot)$. The authors introduce rotation invariance by appending an invariant layer to an equivariant network, where the equivariance becomes invariant by a product of an equivariant signal with the transpose of an equivariant signal. Translation-invariance can be achieved by centering the mean input point cloud at zero and scale-invariance established by scaling each input patch to the size of a unit sphere. These normalization techniques allow us to encode each point cloud into a feature vector z that is invariant to rotation, translation and scale. Additionally, during training we randomly reflect the data along each axis to account for reflectional symmetry. In combination with a rotation invariant encoder, it is sufficient to reflect the data only along one arbitrary axis to learn features robust to reflections.

Contrastive Learning We train the network SymCL to map similar patches (z_i, z_j) close and dissimilar patches (z_i, z_k) far away from each other in the latent space utilizing contrastive learning and the Normalized Temperature-scaled Cross Entropy Loss [32]

$$L_{Xent} = -\log \frac{\exp(sim(z_i, z_j)/\tau)}{\sum_{k=1}^{2N} 1_{[k \neq i]} \exp(sim(z_i, z_k)/\tau)} \quad (6)$$

with cosine-similarity

$$sim(z_i, z_j) = \frac{z_i \cdot z_j}{\|z_i\| \|z_j\|}, \quad (7)$$

where N and τ represent the batch size and the temperature, respectively. Similar patches are defined as a pair of augmented patches originating from the same patch center, whereas dissimilar patches are all other patches within the processed batch. This allows us to learn the network in a

self-supervised manner, where data augmentation provides the supervision signal.

We apply augmentation techniques in the spirit of contrastive learning. First, we apply anisotropic scaling to the data within a range of $[0.8, 1.2]$ for each axis. This allows us to account for small shape and curvature variations. Second, we offset the patch center for which each patch is extracted within a range of $[0.0, 0.1 \cdot \delta_n]$ with respect to the geodesic distance of the original patch center. It allows us to capture the local geometry in a more comprehensive manner, as not only the local curvature is augmented, but also the outline of the patch itself by shifting the border of the patch randomly. Furthermore, it makes our features robust to discretization artifacts.

Supervised Learning Up to this point we described a fully self-supervised method, which is capable of learning robust and descriptive features. Alternatively, we can make use of a supervised training regime. As stated before computing the ICP distances between a large number of patches in infeasible. Instead, we propose to only compute the ICP distances between 64 patches, randomly selected from the full set via FPS (see Sec. 4). Our network (SymML) can then be trained via deep metric learning, to regress the relative cosine similarity of embedded patches $enc(p^{norm}) = z$ in latent space to the relative ICP distance of the original patches p^{norm} in the 3D space. From each batch of patches we construct triplets (p_a, p_i, p_j). Following [12], for each triplet we compute the loss

$$L_{LR} = \left(\log \frac{sim(z_a, z_i)}{sim(z_a, z_j)} - \log \frac{d_{ICP}(p_a, p_i)}{d_{ICP}(p_a, p_j)} \right)^2, \quad (8)$$

where p_a is an anchor patch and p_i, p_j are two other disjunct patches. This allows us to preserve the relative similarity of the patches rather than categorizing them into positive and negative examples.

3.4. Symmetry Detection

To extract symmetry information from an input shape during inference time, we perform the following steps: i) feature selection, ii) aggregation and iii) symmetry extraction.

Feature Selection First, patch centers are selected from the input geometry using FPS. We extract a predefined number of geodesic patches, which are afterwards embedded into the latent space using the trained feature encoder $enc(\cdot)$. We found that using no less than 1000 patches leads to good results.

Aggregation By clustering patches in a rotation, reflection, translation and scale invariant latent space we can aggregate patches exhibiting partial extrinsic symmetries. Each cluster suggests a hypothesis H consisting of multiple regions that are symmetric to each other. Each region $r_i \in H$ is formed by merging several patches. To merge the

patches, it is necessary to identify features $z_j \in H$ that represent contiguous regions $r_i = \{p_{j,0}, ..., p_{j,n}\}$ in 3D space within a symmetry cluster. To achieve this, we cast the clustered features z_j back into the 3D space of the geometry and calculate connected components based on the geodesic distance between the extracted patch centers. In order to revert the effect of FPS, the region r_i is refined by sampling the local neighborhood $\epsilon \ll \delta_d$ of each point of each patch $p_{j,k}$. For clustering, we utilize HDBSCAN [18], a fast and reliable non-parametric clustering algorithm, capable of detecting an a-priori unknown quantity of clusters as well as outliers, representing symmetric or distinctive regions, respectively.

Symmetry Extraction The latent space is only an approximation of the geometric characteristics, and therefore requires filtering. For filtering, we want to evaluate if the detected regions r_i exhibit a symmetric relationship with respect to each other. We can verify this by calculating the ICP distance between all regions of a single hypothesis $r_0, ..., r_n \in H$. The hypothesis is rejected if the greatest distance exceeds a predetermined similarity threshold

$$\delta_{sim} < \max_{r_i \in H, r_j \in H} d_{ICP}(r_i, r_j). \qquad (9)$$

This threshold is fixed to $\delta_{sim} = 0.005$ in our method and also geometrically easily interpretable. Since we assume only a small number of symmetric regions are aggregated within a symmetry cluster, the computation of ICP distances is feasible. We also discard a hypothesis H if it produces a singular region $H = \{r_0\}$ or if more than $n > 30$ regions are detected.

3.5. Symmetry-aware Region Growing

The identified symmetric regions r_i consist of only local patches with limited size that exhibit extrinsic similarity. To complete the symmetric regions we apply a region growing algorithm that partitions the input geometry into maximally symmetric regions r_i^{max}. We process each hypothesis H independently.

For each region $r_i \in H$ we calculate the geodesic distance from the region boundary to all other points sampled from the input geometry. According to its geodesic distance d_{geo}, every point is assigned to the closest region r_i. The largest geodesic distance across all points is denoted as d_{geo}^{max}. Points initially belonging to a region r_i are assigned a distance of 0. To identify the largest symmetric region r_i^{max} we extract regions $r_i^{\delta_d}$, where each point satisfies $d_{geo} \leq \delta_d$ and compute the ICP distance between every pair of regions $r_i^{\delta_d}, r_j^{\delta_d}$. We linearly interpolate δ_d between $[0, d_{geo}^{max}]$ in 100 discrete steps and select the largest symmetric regions r_i^{max} defined by the symmetry threshold

$$\delta_d^{max} = \underset{\delta_d \in [0, d_{geo}^{max}]}{\arg\min} \max_{r_i \in H, r_j \in H} d_{ICP}(r_i^{\delta_d}, r_j^{\delta_d}). \qquad (10)$$

4. Evaluation

In this section, the self-supervised approach SymCL and supervised alternative SymML are evaluated. To assess our method quantitatively, we introduce a novel benchmark test, given the lack of any publicly available extrinsic partial symmetry benchmark. A qualitative comparison is performed on various 3D objects, including classes outside the training set to demonstrate the features' generalizability.

Training We train our models on the training split of PartNet [23]. SymCL is trained with a batch size of 16 for 500 epochs consisting of $10k$ patch pairs each. From each shape in PartNet we sample $[128, 64, 32, 16, 8]$ geodesic patches with a size of $\delta_n = [2^9, 2^{10}, 2^{11}, 2^{12}, 2^{13}]$, respectively, which were randomly shuffled and selected during training. The SymML model is trained on patches with only a size of $\delta_n = 2^{10}$ for which we compute a 64×64 pairwise distance matrix for each shape. The calculation of a single distance matrix requires roughly 105 minutes, which we precompute prior to the training for every shape. A random subset of 16 patches is selected as a batch and the corresponding distance matrix is extracted. Thus, a batch contains only distance values computed on patches originating from the same shape. The model is trained for 50 epochs, processing $10k$ randomly selected shapes in each epoch. The training process is executed on a single RTX 2080Ti GPU and requires 38 and 31 hours for the SymCL and the SymML model, correspondingly.

4.1. Extrinsic Partial Symmetry Benchmarks

To perform a quantitative evaluation of our method we need to define a benchmark test in the first place, as up to our knowledge no publicly available benchmark for partial extrinsic symmetry detection exists. Firstly, we have annotated the PartNet dataset with partial extrinsic symmetry relationships. Secondly, we have established a Pre-Segmented Partial Symmetry Benchmark (PSPSB) and a Partial Symmetry Benchmark (PSB) utilizing this data.

SymPartNet We extend the PartNet dataset [23], comprising 26,671 semantically segmented 3D models across 24 object categories with symmetry annotations at part-level for each model in the test set. We refer to this extended dataset as Symmetry-annotated PartNet (SymPartNet.v1). To assess the similarity of two parts, we compute the ICP distance d_{ICP} between them. Subsequently, we manually choose a threshold δ_{sym} for each shape, which recovers all extrinsic symmetries between the parts. We define two parts with $d_{ICP} \leq \delta_{sym}$ as symmetrical to each other. The annotation process is carried out by a trained worker and each annotation is geometrically inspected through a 3D viewer. For further information, please consult supplementary material Sec. 6.

Benchmarks For PSPSB the goal is to extract an arbitrary number N of symmetric relations between the pre-

5

segmented parts of the input model. The PSB provides only the 3D model without segmentation. The goal is to compute any number N of partitions of the 3D model that contain regions that are symmetric to each other. We utilize the SymPartNet.v1 dataset for both benchmarks and present an example of ground truth data as well as results generated by our method in Fig. 4 and 5. Unlike current intrinsic symmetry benchmarks, our focus is not on establishing one-to-one correspondences between points on surfaces of two related shapes. Instead, we aim to identify symmetry relationships between multiple contiguous regions of the same object.
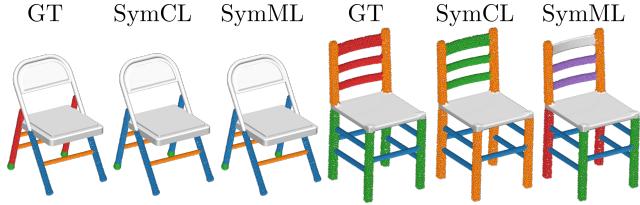

Figure 4. Examples of detected symmetries in PSPSB for chairs. From left to right: ground truth, SymCL, SymML. Colors represent symmetry clusters.
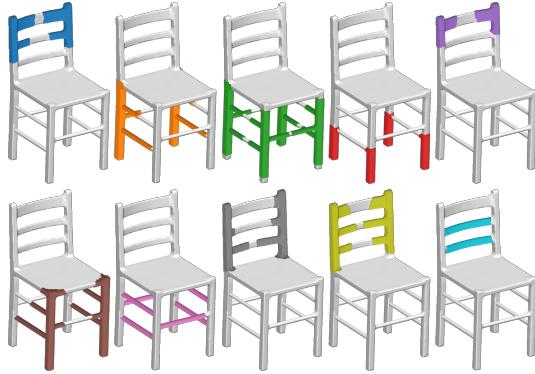

Figure 5. Examples of detected symmetries in PSB for a chair using the SymCL model. Each color represents a symmetry cluster.

Evaluation Metrics The set of previously filtered symmetry hypotheses H (see Sec. 3.4) is now referred to as symmetry set $S = \{H_0, ..., H_n\}$ consisting of symmetry clusters $s_i \in S$. Given a prediction $|S_P| = N$ we calculate three different metrics in each benchmark to evaluate the quality and the faithfulness of the extracted symmetries:

i) The ICP distance (ICP) between every predicted region $r_i \in s_k$ within a symmetry cluster $s_k \in S_P$ estimates how well the extracted symmetries align.

$$\text{ICP} = \frac{1}{|S_P|} \sum_{s_k \in S_P} \max_{r_i \in s_k, r_j \in s_k} d_{ICP}(r_i, r_j) \qquad (11)$$

It is a measure to describe the quality of the extracted symmetries. This measure depends only on the extracted re-

gions within each symmetry cluster and not on the ground truth data.

ii) Intersection over Union (IoU) measures how well the extracted clusters $s_k \in S_P$ align with the extracted ground truth symmetry clusters $s_j \in S_{GT}$.

$$\text{IoU} = \frac{1}{|S_P|} \sum_{s_k \in S_P} \max_{s_j \in S_{GT}} \frac{s_j \cap s_k}{s_j \cup s_k} \qquad (12)$$

To compute it we extract a point cloud with the size of 2^{12} for PSPSB and a size of 2^{16} for PSB and label each point either as an inlier or an outlier of the detected symmetry.

iii) Coverage (COV) measures the fraction of ground truth symmetries S_{GT} that are matched by a predicted symmetry S_P. A match between $s_j \in S_{GT}$ and $s_k \in S_P$ is established if the prediction s_k has the highest IoU for the given symmetry cluster s_j.

$$\text{COV} = \frac{1}{|S_{GT}|} |\{\arg\max_{s_j \in S_{GT}} \frac{s_j \cap s_k}{s_j \cup s_k}\}|, \forall s_k \in S_P \qquad (13)$$

Furthermore, we report the number of models (#Models), which consist of at least one symmetry cluster $|S_P| \geq 1$. All models with no detected symmetry clusters are not considered in the computation of the metrics.

4.2. Quantitative Evaluation

We report the quantitative evaluation metrics for PSPSB and PSB for the SymCL and the SymML model in Tab. 1. For PSB we execute our code on a point cloud of size 2^{16} as described in Sec. 3.4. For PSPSB we only sample a point cloud per part p with size 2^9 and embed it into the latent space $enc(p) = z$. A symmetry relationship between two parts is defined if the cosine similarity of two embedded vectors is smaller than a user-defined threshold $sim(z_i, z_j) \leq \delta_{sym}$. We set δ_{sym} empirically to 0.025 and 0.00025 for SymCL and SymML, respectively. To compute IoU we merge all p and apply FPS to extract a point cloud of size 2^{12}. See supplementary material Sec. 11 for more details.

	PSPSB		PSB	
	SymCL	SymML	SymCL	SymML
ICP ($\downarrow$)	0.0028	0.0018	0.0024	0.0023
IoU ($\uparrow$)	0.7663	0.7783	0.3747	0.3753
COV ($\uparrow$)	0.7727	0.7333	0.8217	0.8293
#Models	969	894	966	965

Table 1. Reported metrics for the Pre-Segmented Partial Symmetry Benchmark (PSPSB) and the Partial Symmetry Benchmark (PSB) for the "Chair" class. The ground truth ICP equals to 0.0017 with 1175 models out of 1217 exhibiting at least one symmetry.

	PSPSB			
	ICP ($\downarrow$)	IoU ($\uparrow$)	COV ($\uparrow$)	#M.
SymCL (base)	0.0028	0.7663	0.7727	969
- offset center	0.0063	0.6846	0.6317	877
- scaling	0.0019	0.7789	0.8031	976
- reflections	0.0023	0.7649	0.7737	976
- multiple sizes	0.0024	0.7582	0.7489	928
Euclidean	0.0025	0.7631	0.7722	965

Table 2. Results of the Pre-Segmented Partial Symmetry Benchmark (PSPSB) leave-one-out ablation for data augmentation.

	PSB			
	ICP ($\downarrow$)	IoU ($\uparrow$)	COV ($\uparrow$)	#M.
SymCL (base)	0.0024	0.3747	0.8217	966
- offset center	0.0022	0.3683	0.7344	863
- scaling	0.0025	0.3412	0.8087	982
- reflections	0.0024	0.3600	0.8207	976
- multiple sizes	0.0024	0.3559	0.839	983
Euclidean	0.0027	0.3446	0.8223	983

Table 3. Results of the Partial Symmetry Benchmark leave-one-out ablation for data augmentation. We see a degradation in quality by removing any augmentation technique.

We see that SymML performs slightly better than SymCL on both benchmarks (see Tab. 1), but the differences are not significant. This shows the encoder is able to learn robust and meaningful features in both cases. Given a segmentation, both models are able to recover 77.27% and 73.33% of the ground truth symmetries with a high IoU of 76.63% and 77.83%, respectively. Even though not all symmetries can be perfectly recovered, the quality of the detected symmetries is very high with an ICP distance of 0.0028 and 0.0018 in comparison to the ground truth with an ICP distance of 0.0017. Note that our networks were trained on patch level inputs instead of parts. In Fig. 4, both methods retrieve valid symmetric relationships between the pre-segmented parts. Notably, the IoU metric for PSB falls behind PSPSB. The disparity can be attributed to the fact that the detected symmetric regions are geometrically motivated and do not always align with the semantic segmentation of the PartNet dataset. In Fig. 5 we observe that all identified symmetries are valid and reasonable solutions to the geometric problem. We argue that our method is able to detect meaningful partial extrinsic symmetries. Unfortunately, since no publicly available implementations of previous partial extrinsic symmetry detection methods exist, we could not report large-scale comparisons to these approaches.

Ablation To assess the impact of different augmentations techniques of the geodesic patches we conduct an ablation study. We evaluate them in a leave-one-out manner and eliminate either the offsetting of the patch center, the anisotropic scaling, reflections or only use single-size patches ($\delta_n = 1024$). Furthermore, we sample patches using the Euclidean instead of the geodesic distance. We report our findings in Tab. 2 and 3.

We see that especially for the PSB the performance degrades in each experiment proving that every data augmentation technique is crucial for the performance of our model. Note how the use of a Euclidean metric to extract patches degrades the performance significantly.

4.3. Qualitative Evaluation

In this subsection we inspect the detected symmetries visually. We also evaluate our method on classes of 3D shapes which were not seen during the training. Additionally, we illustrate the use of the region growing algorithm to expand the identified partial symmetries and generate larger symmetrical regions.

Generalization to Unseen Categories Our method can detect symmetries not only of classes seen during the training, but also of inputs with arbitrary 3D geometry. We demonstrate our results in Fig. 1 where we detect symmetries on *airplanes*, *animals* and *jewelry*, which are classes of objects not contained in PartNet. Our method can retrieve meaningful symmetries. We attribute this due to the fact, that the learning process of our feature extractor is geometrically motivated and focuses on local patches. Thus, the learned geometric features can be carried over to other unseen categories of geometry.

Symmetry-aware Region Growing We apply the region growing algorithm to the detected partial symmetries and present the results in Fig. 1 and 6. The region growing algorithm is able to maximize the regions of detected partial symmetries. Note, in some cases we do not partition the whole shape into symmetric regions, as this would break the found symmetric relationships between the regions. This represents a significant contrast to segmentation, in which the objective is to divide the entire shape into multiple disjunct regions. In our approach, we do not impose such limitations. As the problem of partial symmetry detection is inherently ambiguous, we aim to retrieve all valid solutions and enable our method to generate multiple, potentially partial, partitions of the input 3D shape.

In Fig. 6, we illustrate the development of the ICP distance throughout the completion of a symmetric region. To obtain maximal regions that remain symmetrical to each other, we establish $\delta_d = 0.01$ as a suitable compromise between accurate symmetries and expansive regions. For various symmetries, distinct partitions of the shape are ac-
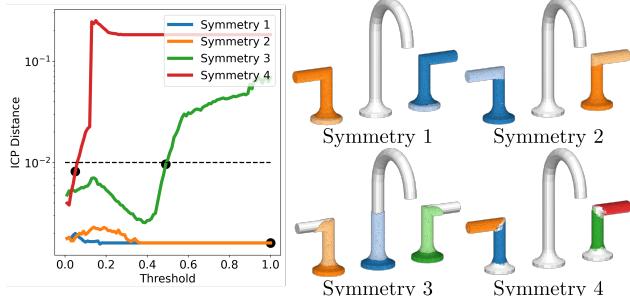
Figure 6. Development of the ICP distance during the region growing process. The largest region for each symmetry is chosen with a threshold of $\delta_d = 0.01$.
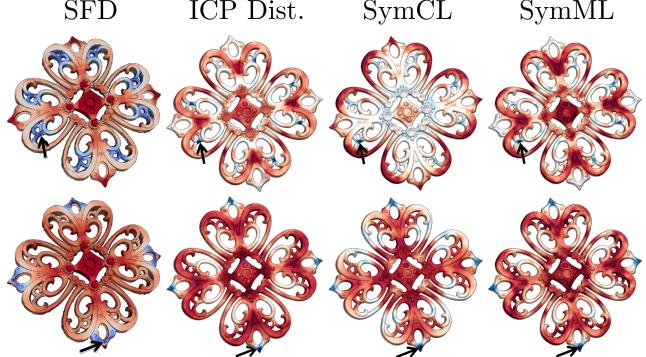

Figure 7. Visualization of Symmetry Factored Distance [16] and distances defined by SymCL and SymML as well as the ICP distance measured from points marked by black arrows. Blue represents close distances and red large ones. Note how our model is able to detect similar features more localized at the sample points. Features learned by our encoder are geometrically interpretable.

quired. For both *Symmetry 1* and *2*, the faucet handles are fully completed. Note how the ICP distance is minimized during the region growing process. In contrast, initially comprising three bases, *Symmetry 3* has the capability to extend along the pipes until the handles cause a disruption in the symmetry. The detected *Symmetry 4* is already almost maximal, as any further region growing leads to an increased ICP distance.

4.4. Comparison to Symmetry Factored Distance

We conduct a qualitative comparison of the Symmetry Factored Distance (SFD) [16] with distances defined by SymCL and SymML. Additionally, we calculate the ICP distance for each sampled patch. The results are visualized in Fig. 7. We see that SymCL and SymML detect similar features more localized at the sample points rather than in SFD. We can interpret the extracted features of our encoder geometrically. Symmetric patterns are recognized in all examples, indicating that the extracted features indeed represent symmetrical structures. Unfortunately, the comparison to SFD can be made only relative, as we do not know the color range nor have access to a publicly available implementation of the method. Significantly, the computation of the full ICP distance matrix requires approximately 48 hours, whereas our method's embedding of the patches and calculation of the distance matrix take only 54 seconds.

5. Conclusion

We propose a novel method for the task of extrinsic partial symmetry detection, utilizing either a self-supervised model or a supervised alternative. Our approach can detect an arbitrary number of valid solutions for an ambiguous and challenging problem. Combining data-driven methods with conventional model-driven algorithms allows us to geometrically interpret intermediate computations in each step of our pipeline. Additionally, we present a newly developed benchmark test to evaluate the accuracy of detecting extrinsic partial symmetries and enable comparison among dif-

ferent techniques in the future. The ablation study demonstrates that employing geodesic patches with the proposed augmentations significantly enhances the quality of identified symmetries. This result is likely to be valuable for other point cloud-based 3D deep learning applications and the use of local geodesic patches could potentially enhance the performance of other techniques that benefit from structure-aware information.

Limitations and Future Work The detection of symmetry is geometrically driven, but the partitioning of the PartNet dataset is based on semantics. Consequently, there is a possibility that the annotations of SymPartNet may not encompass all feasible solutions, or even introduce a bias into the ground truth. Currently, the benchmarks are only evaluated on the *chair* subset of SymPartNet, as we are in the process of finishing the annotations for all classes. Still, we show qualitative examples for many classes, even ones not seen during the training of our model. An evaluation with approximated thresholds δ_{sym}^{cls} for all classes can be found in supplementary material Sec. 9. We do expect only minor variations in the updated metrics. We could not remove all thresholds from our method and a single threshold δ_{sim} to filter the symmetry hypothesis remains. Nevertheless, this threshold is geometrically motivated, easily interpretable and fixed for all input shapes to a single value. The presented region growing algorithm allows only for equidistant growing of patches. It would be of high interest to research an alternative to allow each patch to grow at an individual rate to minimize the ICP distance between the regions even further.

References

[1] Atallah. On symmetry detection. *IEEE Transactions on Computers*, 100(7):663–666, 1985. 2

[2] Paul J Besl and Neil D McKay. Method for registration of 3-d shapes. In *Sensor fusion IV: control paradigms and data structures*, pages 586–606. Spie, 1992. 3

[3] Martin Bokeloh, Alexander Berner, Michael Wand, H-P Seidel, and Andreas Schilling. Symmetry detection using feature lines. In *Comput. Graph. Forum*, pages 697–706. Wiley Online Library, 2009. 2

[4] Keenan Crane, Clarisse Weischedel, and Max Wardetzky. The heat method for distance computation. *Communications of the ACM*, 60(11):90–99, 2017. 3

[5] Congyue Deng, Or Litany, Yueqi Duan, Adrien Poulenard, Andrea Tagliasacchi, and Leonidas J Guibas. Vector neurons: A general framework for so (3)-equivariant networks. In *ICCV*, pages 12200–12209, 2021. 4

[6] Haoqiang Fan, Hao Su, and Leonidas J Guibas. A point set generation network for 3d object reconstruction from a single image. In *CVPR*, pages 605–613, 2017. 3

[7] Ran Gal and Daniel Cohen-Or. Salient geometric features for partial shape matching and similarity. *ACM Transactions on Graphics (TOG)*, 25(1):130–150, 2006. 2

[8] Lin Gao, Jie Yang, Tong Wu, Yu-Jie Yuan, Hongbo Fu, Yu-Kun Lai, and Hao Zhang. Sdm-net: Deep generative network for structured deformable mesh. *ACM TOG*, 38(6):1–15, 2019. 2

[9] Lin Gao, Ling-Xiao Zhang, Hsien-Yu Meng, Yi-Hui Ren, Yu-Kun Lai, and Leif Kobbelt. Prs-net: Planar reflective symmetry detection net for 3d models. *IEEE TVCG*, 27(6): 3007–3018, 2020. 2

[10] Penglei Ji and Xinguo Liu. A fast and efficient 3d reflection symmetry detector based on neural networks. *Multimedia Tools and Applications*, 78:35471–35492, 2019. 2

[11] Michael Kazhdan, Bernard Chazelle, David Dobkin, Thomas Funkhouser, and Szymon Rusinkiewicz. A reflective symmetry descriptor for 3d models. *Algorithmica*, 38:201–225, 2004. 2

[12] Sungyeon Kim, Minkyo Seo, Ivan Laptev, Minsu Cho, and Suha Kwak. Deep metric learning beyond binary supervision. In *Proceedings of the IEEE/CVF Conference on Computer Vision and Pattern Recognition*, pages 2288–2297, 2019. 4

[13] Bo Li, Henry Johan, Yuxiang Ye, and Yijuan Lu. Efficient 3d reflection symmetry detection: A view-based approach. *Graphical Models*, 83:2–14, 2016. 2

[14] Jun Li, Kai Xu, Siddhartha Chaudhuri, Ersin Yumer, Hao Zhang, and Leonidas Guibas. Grass: Generative recursive autoencoders for shape structures. *ACM TOG*, 36(4):1–14, 2017. 2

[15] Ren-Wu Li, Ling-Xiao Zhang, Chunpeng Li, Yu-Kun Lai, and Lin Gao. E3sym: Leveraging e (3) invariance for unsupervised 3d planar reflective symmetry detection. In *ICCV*, pages 14543–14553, 2023. 2

[16] Yaron Lipman, Xiaobai Chen, Ingrid Daubechies, and Thomas Funkhouser. Symmetry factored embedding and distance. *ACM TOG*, 2010. 2, 8

[17] Aurélien Martinet, Cyril Soler, Nicolas Holzschuch, and François X Sillion. Accurate detection of symmetries in 3d shapes. *ACM TOG*, 25(2):439–464, 2006. 2

[18] Leland McInnes, John Healy, and Steve Astels. hdbscan: Hierarchical density based clustering. *The Journal of Open Source Software*, 2(11):205, 2017. 5

[19] Niloy J Mitra, Leonidas J Guibas, and Mark Pauly. Partial and approximate symmetry detection for 3d geometry. *ACM TOG*, 25(3):560–568, 2006. 2

[20] Niloy J Mitra, Alex Bronstein, and Michael Bronstein. Intrinsic regularity detection in 3d geometry. In *Computer Vision–ECCV 2010: 11th European Conference on Computer Vision, Heraklion, Crete, Greece, September 5-11, 2010, Proceedings, Part III 11*, pages 398–410. Springer, 2010. 2

[21] Niloy J Mitra, Mark Pauly, Michael Wand, and Duygu Ceylan. Symmetry in 3d geometry: Extraction and applications. In *Comput. Graph. Forum*, pages 1–23. Wiley Online Library, 2013. 2

[22] Kaichun Mo, Paul Guerrero, Li Yi, Hao Su, Peter Wonka, Niloy Mitra, and Leonidas Guibas. Structurenet: Hierarchical graph networks for 3d shape generation. *ACM TOG*, 38 (6):Article 242, 2019. 2, 1

[23] Kaichun Mo, Shilin Zhu, Angel X Chang, Li Yi, Subarna Tripathi, Leonidas J Guibas, and Hao Su. Partnet: A large-scale benchmark for fine-grained and hierarchical part-level 3d object understanding. In *Proceedings of the IEEE/CVF conference on computer vision and pattern recognition*, pages 909–918, 2019. 5, 1

[24] Rajendra Nagar and Shanmuganathan Raman. Fast and accurate intrinsic symmetry detection. In *ECCV*, pages 417–434, 2018. 2

[25] Maks Ovsjanikov, Jian Sun, and Leonidas Guibas. Global intrinsic symmetries of shapes. In *Computer graphics forum*, pages 1341–1348. Wiley Online Library, 2008. 2

[26] M. Pauly, N. J. Mitra, J. Wallner, H. Pottmann, and L. Guibas. Discovering structural regularity in 3D geometry. *ACM Transactions on Graphics*, 27(3):#43, 1–11, 2008. 2

[27] Joshua Podolak, Philip Shilane, Aleksey Golovinskiy, Szymon Rusinkiewicz, and Thomas Funkhouser. A planar-reflective symmetry transform for 3D shapes. *ACM TOG*, 25(3), 2006. 2

[28] Charles Ruizhongtai Qi, Li Yi, Hao Su, and Leonidas J Guibas. Pointnet++: Deep hierarchical feature learning on point sets in a metric space. *Advances in neural information processing systems*, 30, 2017. 3

[29] Yi-Ling Qiao, Lin Gao, Shu-Zhi Liu, Ligang Liu, Yu-Kun Lai, and Xilin Chen. Learning-based intrinsic reflectional symmetry detection. *IEEE TVCG*, 2022. 2

[30] Nicholas Sharp, Keenan Crane, et al. Geometrycentral: A modern c++ library of data structures and algorithms for geometry processing. 2019. 3

[31] Ivan Sipiran, Robert Gregor, and Tobias Schreck. Approximate symmetry detection in partial 3d meshes. In *Computer Graphics Forum*, pages 131–140. Wiley Online Library, 2014. 2

[32] Kihyuk Sohn. Improved deep metric learning with multi-class n-pair loss objective. *NeurIPS*, 29, 2016. 4

[33] Hui Wang and Hui Huang. Group representation of global intrinsic symmetries. In *Comput. Graph. Forum*, pages 51–61. Wiley Online Library, 2017. 2

[34] Kai Xu, Hao Zhang, Andrea Tagliasacchi, Ligang Liu, Guo Li, Min Meng, and Yueshan Xiong. Partial intrinsic reflectional symmetry of 3d shapes. In *ACM SIGGRAPH Asia 2009 papers*, pages 1–10. 2009. 2

[35] Kai Xu, Hao Zhang, Wei Jiang, Ramsay Dyer, Zhiquan Cheng, Ligang Liu, and Baoquan Chen. Multi-scale partial intrinsic symmetry detection. *ACM TOG*, 31(6):1–11, 2012. 2

[36] Jie Yang, Kaichun Mo, Yu-Kun Lai, Leonidas J Guibas, and Lin Gao. Dsg-net: Learning disentangled structure and geometry for 3d shape generation. *ACM TOG*, 42(1):1–17, 2022. 2

[37] Fenggen Yu, Kun Liu, Yan Zhang, Chenyang Zhu, and Kai Xu. Partnet: A recursive part decomposition network for fine-grained and hierarchical shape segmentation. In *CVPR*, pages 9491–9500, 2019. 2

Partial Symmetry Detection for 3D Geometry using Contrastive Learning with Geodesic Point Cloud Patches

Supplementary Material

6. Symmetry-annotated PartNet

The annotation of the SymPartNet dataset, which is based on PartNet [23], is performed by a trained worked. In this chapter we describe the annotation process in more detail.

Firstly, given a segmented 3D shape, we compute the ICP distance between each part of the shape. The ICP distance describes the geometric similarity of two 3D shapes after their registration. Thus, it is able to describe the similarity of two parts independent of their position, rotation or reflection. The result is a distance matrix for each shape. Secondly, we inspect each shape independently in our annotation tool visualized in Fig. 8. For each shape we select a threshold, which implicitly transforms the computed similarity information into annotated symmetry annotation. In this way we do not need to annotate each pair of parts and only annotate a single value. This speeds up the annotation process and limits inconsistencies across a single shape. Thirdly, to extract the symmetry information between multiple parts we compute connected components on the thresholded distance matrix. All parts belonging to the same connected component are visualized in the same color in the annotation tool. Additionally, the user can change the view to visualize only a single symmetry component in which every part is visualized in a different color to allow for better differentiation and more accurate annotations. Lastly, after a threshold is selected and evaluated, it is saved next to the distance matrix.
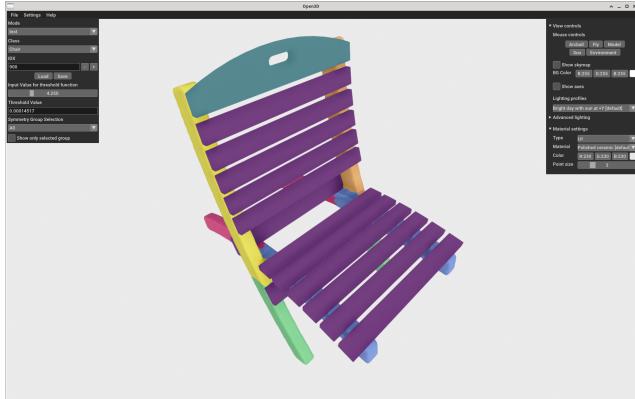

Figure 8. View of our annotation tool to inspect each shape independently. The user can select a symmetry threshold which translates the similarity matrix into a symmetry matrix. Each group of symmetric parts is shown in the same color. The shape can be freely rotated and inspected from each direction.

7. ICP-Distance Evaluation

We evaluate the quality of the previously introduced ICP distance. For this experiment we choose either 500 random patches, parts or shapes from the PartNet dataset and register a copy of each shape onto itself. In each iteration the orientation of the shape is randomly initialized, to simulate the unknown optimal registration. A parameter which needs to be chosen for the ICP distance is the number of iterations N from which the best registration is chosen. Fig. 9 reports the results, where we plot the mean ICP distance as well as the standard deviation across 500 independent registrations over the iterations. We see that with an increasing number of iterations, the distance converges towards zero. As a trade-off between speed and accuracy we decided to select $N = 30$. We can observe different behavior of the ICP distance for different instances. It converges the fastest for parts, as they have the most simple geometric point clouds, mostly consisting of elongated cylinders or quadratic shapes, which have multiple planes of symmetry, where multiple solutions with a minimal ICP distance exist. We need to find only a single solution to obtain the minimal distance. For patches there exists mostly a single solution with a minimal distance. Thus, they converge slower. Shapes have the most complex geometry. Their registrations yield very bad distance values at the beginning, as they are highly dependent on a good initial solution to converge. After finding an approximately good initial solution, the ICP algorithm is able to quickly find the optimal registration, resulting in a minimal ICP distance.

8. Symmetry Detection using StructureNet

In Sec. 2 we state that StructureNet [22] describes a way to decode structural information from an input point cloud which can be encoded into a corresponding latent space. This structural information incorporates edges between bounding boxes, which describe relationships like rotational, translational or reflective symmetry. We show in Fig. 10 four randomly selected examples for shapes encoded and decoded from the train and test set each. Note how only the shapes from the train set align well with the decoded structure. In the test set only the seats align with the shape and all other parts, like legs, armrests or the back of the chair misalign or miss entirely. As the published code does not include the pretrained weights to embed a point cloud into the latent space of the decoder, nor the code to train such a model was released, we had to reimplement
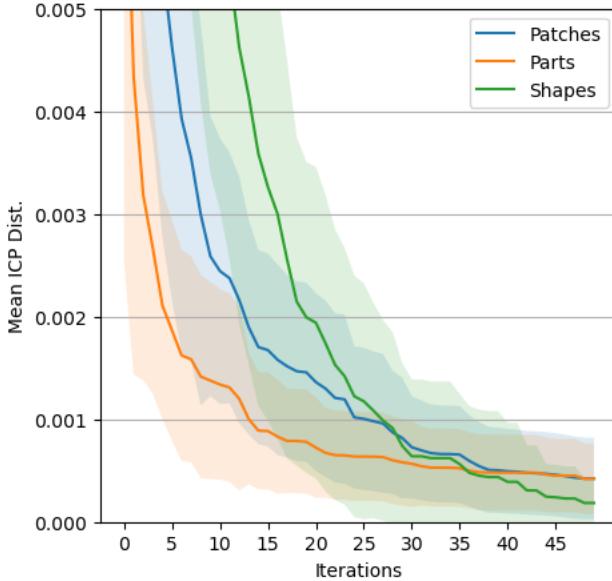
Figure 9. Mean and standard deviation of the ICP distance over iterations. Experiment performed on 500 randomly selected patches, parts and shapes from PartNet, where each element is registered onto itself given a random initialization of the rotation. Note how the algorithm gradually converges over the iterations.
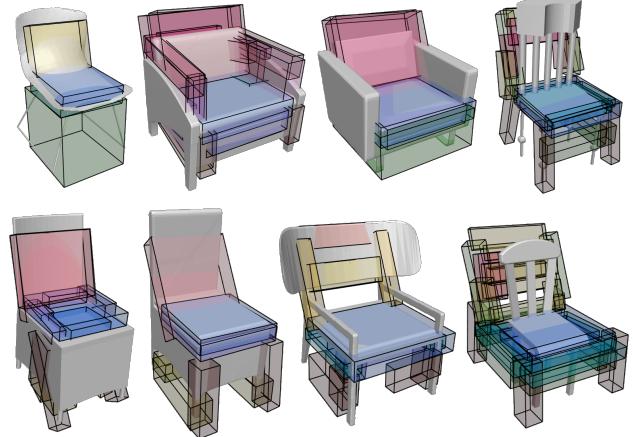

Figure 10. Results generated by StructureNet using a point cloud encoder and decoding the latent space by a pre-trained decoder. We overlay the decoded boxes representing the learned structure with the input shape. The top row shows examples from the training set, the bottom row is evaluated on examples from the test set. Note how only the examples from the train set align well with the input shape. Especially on examples from the test set, legs or armrest cannot be decoded and aligned faithfully.

this method ourselves. Due to the poor qualitative performance of the model in extracting structure and symmetry from a point cloud, we refrain from a quantitative evaluation or comparison to our method. Additionally, we cannot guarantee an errorless reverse engineering of this method. Furthermore, an evaluation of it on PSB would require an additional mapping of the decoded bounding boxes onto the surface of the input shape. This step would include adjustments to StructureNet not described by the authors introducing possibly unintended inaccuracies. In contrast, our method works directly on a sampled point cloud classifying points into symmetry clusters. Our method has a perfect alignment to the input geometry by default.

9. Quantitative Evaluation per Class

In Tab. 7 and 8 we report results of the Pre-Segmented Partial Symmetry Benchmark (PSPSB) and in Tab. 5 and 6 the results for the Partial Symmetry Benchmark (PSB) using approximated annotations for each of our models SymML and SymCL, respectively. We skip all objects consisting of more than 30 parts in the benchmark. Note, the metrics for the *chair* class are worse on this approximated annotations than the metrics on the manually annotated data reported in the main paper (cmp. Tab. 1). We expect the same behavior for all other classes after finishing the annotation process and rerunning the benchmarks. For each class we annotate 5 randomly selected objects and compute the mean similarity

threshold. Afterwards we use this threshold for all objects of the same class to extract the ground truth symmetries.

10. Additional Examples

We provide additional examples for the Pre-Segmented Partial Symmetry Benchmark (PSPSB) and the Partial Symmetry Benchmark (PSB) in Fig. 11 and 12, respectively. For some objects we detect more than six symmetries, but only show up to six symmetry clusters in the figure as the other symmetries are very similar to the already shown ones.

11. Threshold selection for PSPSB

To evaluate our models on PSPSB we have to define a symmetry threshold δ_{sym}, which sets a value to translate similarity in latent space into a symmetry relationship of two embedded parts $sim(z_i, z_j) \leq \delta_{sym}$. We perform a short study of different values and select 0.025 and 0.00025 for the SymCL and the SymML model empirically. Results of our experiments are reported in Table. We aimed at a possible largest IoU value, to account for the best alignment of the detected symmetries to the ground truth. All experiments were performed on the *chair* subset of SymPartNet.
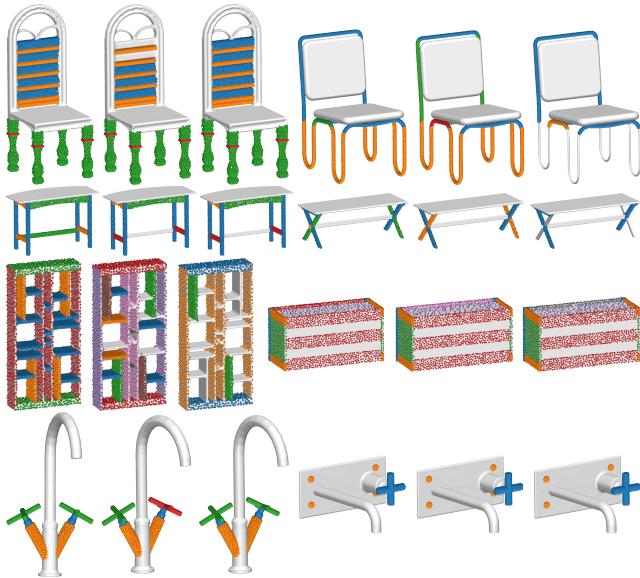
Figure 11. Additional examples for the Pre-Segmented Partial Symmetry Benchmark (PSPSB) for the classes *chair*, *table*, *storage furniture* and *faucet*. From left to right: ground truth, SymCL and SymML. Each color represents a symmetry cluster.

δ_{sym}	ICP ($\downarrow$)	IoU ($\uparrow$)	COV ($\uparrow$)	#M.
PSPSB Threshold				
SymCL				
0.1	0.0159	0.6548	0.7707	1023
0.05	0.0066	0.7369	0.8173	1017
0.025	0.0034	0.7544	0.7789	987
0.01	0.0025	0.7107	0.6284	828
SymML				
0.001	0.0036	0.7331	0.7396	975
0.0005	0.0025	0.7586	0.7588	970
0.00025	0.0020	0.7723	0.7507	932
0.0001	0.0013	0.7616	0.6990	847

Table 4. Results for Pre-Segmented Partial Symmetry Benchmark (PSPSB) using different symmetry thresholds δ_{sym}. We select the threshold with the best IoU to account for best alignment of the detected symmetries to the ground truth. Each color represents a symmetry cluster. Detected symmetries may overlap, thus we render each symmetry cluster separately.

Figure 12. Additional examples for the Partial Symmetry Benchmark (PSB) for the classes *chair*, *table*, *storage furniture* and *faucet*. We show up to six detected symmetries for each model. Each color represents a symmetry cluster.

	PSB - SymML					**PSB - SymCL**			
	ICP ($\downarrow$)	IoU ($\uparrow$)	COV ($\uparrow$)	#M.		ICP ($\downarrow$)	IoU ($\uparrow$)	COV ($\uparrow$)	#M.
bag	0.0023	0.2785	0.9091	22	*bag*	0.0025	0.2240	0.9127	21
bed	0.0029	0.0996	0.5718	12	*bed*	0.0028	0.0996	0.4294	18
bottle	0.0032	0.0445	0.9914	58	*bottle*	0.0030	0.0429	1.0000	45
bowl	0.0032	0.1938	1.0000	9	*bowl*	0.0030	0.0985	1.0000	7
chair	0.0022	0.3474	0.8700	954	*chair*	0.0024	0.3480	0.8749	957
clock	0.0029	0.1549	0.8356	74	*clock*	0.0027	0.1064	0.8683	62
dishwasher	0.0039	0.0038	0.7760	16	*dishwasher*	0.0034	0.0050	0.8333	25
display	0.0031	0.0736	0.9612	67	*display*	0.0029	0.0707	0.9437	64
door	0.0026	0.2317	0.8352	35	*door*	0.0025	0.1935	0.8295	35
earphone	0.0030	0.3110	0.7274	27	*earphone*	0.0028	0.2534	0.6594	24
faucet	0.0030	0.2646	0.8245	64	*faucet*	0.0030	0.2758	0.8219	61
hat	0.0028	0.0118	1.0000	9	*hat*	0.0030	0.0079	1.0000	8
keyboard	-	-	-	0	*keyboard*	-	-	-	0
knife	0.0025	0.1278	0.8681	12	*knife*	0.0024	0.0606	0.9259	9
lamp	0.0027	0.1433	0.8691	202	*lamp*	0.0026	0.1555	0.8837	190
laptop	-	-	-	0	*laptop*	-	-	-	0
microwave	0.0034	0.0150	0.8654	13	*microwave*	0.0032	0.0089	0.7731	18
mug	-	-	-	0	*mug*	-	-	-	0
refrigerator	0.0036	0.0257	0.7381	7	*refrigerator*	0.0031	0.0276	0.7917	12
scissors	0.0024	0.2585	0.8788	11	*scissors*	0.0021	0.3292	0.8333	10
storagefurnit.	0.0031	0.3937	0.5272	168	*storagefurnit.*	0.0031	0.3877	0.5239	181
table	0.0024	0.3693	0.8926	1334	*table*	0.0024	0.3769	0.8787	1349
trashcan	0.0034	0.1576	0.8094	23	*trashcan*	0.0032	0.1182	0.8213	25
vase	0.0028	0.1570	0.8266	37	*vase*	0.0029	0.1910	0.7623	34
All	0.0025	0.3155	0.8603	3154	*All*	0.0025	0.3186	0.8522	3155

Table 5. Reported metrics for the Partial Symmetry Benchmark (PSB) and the SymML model for all classes of SymPartNet using approximated thresholds.

Table 6. Reported metrics for the Partial Symmetry Benchmark (PSB) and the SymCL model for all classes of SymPartNet using approximated thresholds.

	PSPSB - SymML					PSPSB - SymCL			
	ICP ($\downarrow$)	IoU ($\uparrow$)	COV ($\uparrow$)	#M.		ICP ($\downarrow$)	IoU ($\uparrow$)	COV ($\uparrow$)	#M.
bag	0.0013	0.5877	0.8889	12	*bag*	0.0030	0.6697	0.8627	17
bed	0.0015	0.8100	0.5901	17	*bed*	0.0031	0.8159	0.6059	15
bottle	0.0029	0.2080	1.0000	2	*bottle*	0.0062	0.5022	1.0000	7
bowl	0.0017	0.7680	1.0000	5	*bowl*	0.0017	0.7100	1.0000	4
chair	0.0017	0.6721	0.8087	895	*chair*	0.0027	0.6622	0.8449	967
clock	0.0018	0.4458	0.7323	33	*clock*	0.0041	0.4494	0.7154	41
dishwasher	0.0017	0.5390	0.8287	18	*dishwasher*	0.0045	0.5948	0.9430	19
display	0.0022	0.6483	0.9184	38	*display*	0.0038	0.6038	0.9024	42
door	0.0013	0.7232	0.8138	29	*door*	0.0065	0.6490	0.7932	22
earphone	0.0020	0.7295	0.7218	22	*earphone*	0.0034	0.7097	0.8737	28
faucet	0.0021	0.6458	0.6897	42	*faucet*	0.0053	0.6525	0.8842	60
hat	0.0011	0.4844	1.0000	3	*hat*	0.0025	0.7912	1.0000	5
keyboard	-	-	-	0	*keyboard*	-	-	-	0
knife	0.0015	0.7882	0.6771	8	*knife*	0.0040	0.7708	0.7500	6
lamp	0.0015	0.7801	0.8161	157	*lamp*	0.0029	0.7638	0.8878	177
laptop	0.0014	0.4810	0.7422	32	*laptop*	0.0035	0.3981	0.7448	32
microwave	0.0021	0.7193	0.8864	22	*microwave*	0.0030	0.6662	0.9133	25
mug	-	-	-	0	*mug*	-	-	-	0
refrigerator	0.0014	0.8752	0.7750	10	*refrigerator*	0.0036	0.7373	0.9394	11
scissors	0.0012	0.9239	0.6354	8	*scissors*	0.0025	0.7898	0.6759	9
storagefurnit.	0.0015	0.6873	0.7356	219	*storagefurnit.*	0.0027	0.6217	0.6616	210
table	0.0014	0.7680	0.8188	1289	*table*	0.0021	0.7501	0.8051	1324
trashcan	0.0017	0.7293	0.6233	10	*trashcan*	0.0045	0.6987	0.8048	14
vase	0.0012	0.7212	0.8939	33	*vase*	0.0020	0.8080	0.9213	36
All	0.0016	0.7193	0.8054	2904	*All*	0.0026	0.7000	0.8176	3071

Table 7. Reported metrics for the Pre-Segmented Partial Symmetry Benchmark (PSPSB) and the SymML model for all classes of SymPartNet for approximated thresholds.

Table 8. Reported metrics for the Pre-Segmented Partial Symmetry Benchmark (PSPSB) and the SymCL model for all classes of SymPartNet for approximated thresholds.